Effects of Size Polydispersity and Dense Media on Quantitative Ultrasound Estimates

Olivier Lombard, Emilie Franceschini

Effects of size polydispersity and dense media on quantitative ultrasound estimates

Olivier Lombard, Emilie Franceschini
Aix-Marseille Univ, CNRS, Centrale Marseille, LMA, Turing Centre for Living Systems, Marseille, France

***Abstract*—Quantitative ultrasound (QUS) techniques based on the backscatter coefficient (BSC) aim to characterize the scattering properties of biological tissues. A scattering model is fit to the measured BSC and the fitted QUS parameters can provide local tissue microstructure, namely scatterer size and acoustic concentration. However, these techniques may fail to provide a correct description of tissue microstructure when the medium is polydisperse and/or dense. The objective of this study is to investigate the effects of scatterer size polydispersity in sparse or dense media on the QUS estimates. Four scattering models (*i.e.* the monodisperse and polydisperse sparse models, and the monodisperse and polydisperse concentrated models based on the structure factor) are compared to assess their accuracy and reliability in quantifying the QUS estimates. Simulations are conducted with different scatterer size distributions for sparse, moderately dense and dense media (volume fractions of 1%, 20% and 73%, respectively). The QUS parameters are estimated by using model-based inverse methods at different center frequencies between 8 MHz and 50 MHz. Experimental data are also analyzed using colon adenocarcinoma HT29 cell pellet biophantoms to further validate the results obtained from simulations at the volume fraction of 73%. Our findings reveal that the choice of scattering model has a significant impact on the accuracy of QUS estimates. For sufficiently high frequencies and dense media, the polydisperse concentrated model outperforms the other models and enables more accurate quantification. Furthermore, our results contribute to advancing our understanding of the complexities associated with scatterer size polydispersity and dense media in spectral-based QUS techniques.**

Simulations are conducted with different scatterer size distributions for sparse, moderately dense and dense media (volume fractions of 1%, 20% and 73%, respectively). The QUS parameters are estimated by using model-based inverse methods at different center frequencies between 8 MHz and 50 MHz. Experimental data are also analyzed using colon adenocarcinoma HT29 cell pellet biophantoms to further validate the results obtained from simulations at the volume fraction of 73%. Our findings reveal that the choice of scattering model has a significant impact on the accuracy of QUS estimates. For sufficiently high frequencies and dense media, the polydisperse concentrated model outperforms the other models and enables more accurate quantification. Furthermore, our results contribute to advancing our understanding of the complexities associated with scatterer size polydispersity and dense media in spectral-based QUS techniques.

I. Introduction

The spectral-based quantitative ultrasound (QUS) techniques aim to differentiate between healthy and pathological tissues, detect cancers or monitor tumor response to treatment [1]. These techniques are based on the analysis of the spectral content of signals backscattered from tissues, and more specifically on the analysis of frequency-dependent backscatter coefficient (BSC) (which is defined as the power backscattered by a unit volume of scatterers per unit incident intensity per unit solid angle). The BSC is a fundamental property of tissue similar to the sound speed and attenuation of tissue, and is a system-independent and operator-independent quantity. Most of QUS techniques are model-based. A theoretical scattering model is fit to the measured BSC in order to estimate the fitted parameters, termed QUS estimates. These QUS estimates are used to characterize the scattering properties of the tissue under investigation related to the underlying tissue microstructure. The most widely used scattering models are the spherical Gaussian model [2] that describes tissues as a random inhomogeneous continuum with acoustic impedance fluctuations, and the fluid-filled sphere model [3] that considers tissue as an ensemble of discrete spherical scatterers. Both the spherical Gaussian model and the fluid-filled sphere model assume sparse scattering media and yield two QUS estimates: the effective scatterer radius a and the effective acoustic concentration n_z, defined as the product of the scatterer number density and the square of the relative acoustic impedance difference between the scatterers and the surrounding medium [4]. The effective scatterer size corresponds to the correlation length of impedance fluctuations when using the continuous scattering model, or to the characteristic size of scatterers when using the discrete scattering model.

However, the estimation of a single-scatterer size may not be representative of the actual tissue microstructure, since biological tissues often have structures of many sizes. Roberjot et al. [5] and Mamou et al. [6] studied sparse scattering media containing two-population sizes of scatterers and estimated the effective scatterer size by using single-size models. They demonstrated that scatterer size estimates vary depending upon the chosen frequency bandwidth [5], and that the smaller scatterers are resolved only when the number density or acoustic impedance contrast of the smaller scatterers is much larger than that of the larger scatterers [6]. Lavarello & Oelze [7] showed that single-size scattering models may not provide the size of actual physical structures when the medium under investigation contains sparse scatterers whose sizes follow a continuous probability density function (PDF). Strategies based on different estimator algorithms can help in reducing the effects of scatterer size distribution on the final single-size estimate [8]. Other strategies are more model-based to characterize polydisperse media. Nordberg and Hall [9] suggested the use of an exponential form factor to identify

the presence of broad scatterer distribution, and demonstrated that the single-size exponential form factor model provides better fit to the simulated data from broad polydisperse media when compared to the single-size Gaussian form factor model. Jafarpisheh et al. [10] proposed to use the linear combination of single-size form factors to account for any scatterer size distribution and directly estimate the size distribution from simulated data. The aforementioned model-based approaches [2]–[4], [9], [10] assume sparse media and are not adapted to model concentrated media such as densely packed cells in tumors. Another class of scattering models consider the combined effects of scatterer size polydispersity and dense media, like the concentrated structure factor model (SFM) [11]–[13]. The concentrated SFM describes tissue as an ensemble of discrete scatterers and models the interference effects caused by correlations among scatterers' positions (*i.e.* caused by coherent scattering) with a structure factor. The polydisperse concentrated SFM parameterizes the BSC with four parameters: the mean scatterer size $\bar{a}^*$, the standard deviation SD^*, the volume fraction ϕ^* and the relative acoustic impedance contrast γ_z^* (and only three parameters in the special case of the monodisperse concentrated SFM). The polydisperse concentrated SFM was used to explain the increase in BSC amplitude of cell biophantoms caused by an increase in cellular size variance during chemotherapy [12], [13]. The combination of the polydisperse concentrated SFM with an effective medium theory was proposed to estimate the polydispersity in size of aggregates of red blood cells in flowing blood [14]. Franceschini et al. [15] compared the performance of two sparse models (*i.e.*, Gaussian model, fluid-filled sphere model) and the concentrated SFM to estimate scatterer size and acoustic concentration from simulations and experiments on cell pellet biophantoms with a range of scatterer volume fractions. Results demonstrated the superiority of the concentrated SFM[1] over sparse models for the narrow size distribution studied. Although it is now well established that the concentrated SFM outperforms sparse models in characterizing dense media, caution should be exercised in interpreting QUS estimates, as inaccurate models and/or an inappropriate frequency range can result in unreliable QUS estimates [5]–[8]. Little attention has been paid to the influence of broad scatterer size distribution on scatterer size estimates when considering dense media. Our preliminary simulation results [16] showed biases in the scatterer size estimated with the sparse models or with the monodisperse concentrated SFM for highly polydisperse media at volume fractions of 1% and 20%. The work proposed here extends this preliminary study to more dense media by considering both simulated and experimental data. Moreover, the performance of the polydisperse concentrated SFM to estimate QUS parameters is studied for the first time.

The goal of the present work is to study the effects of scatterer size polydispersity on QUS estimates for sparse or dense media by considering four scattering models: the monodisperse and polydisperse sparse models, and the monodisperse and polydisperse concentrated SFM. The performance of scattering models to estimate QUS parameters was investigated by simulations and experiments for different frequency ranges. Controlled simulations of BSCs were conducted with different scatterer size distributions for sparse, moderately dense and dense media (volume fractions of 1%, 20% and 73%, respectively). The QUS estimates are obtained by fitting the simulated BSC with one of the four scattering models at different center frequencies f_0 from 8 MHz up to 50 MHz. Experimental data were also considered using colon adenocarcinoma HT29 cell pellet biophantoms to further validate the results obtained from simulations at the volume fraction of 73%.

[1]Note that in this work [15], both monodisperse and polydisperse concentrated SFM were examined. When using the polydisperse concentrated SFM, the whole cell size variance was assumed to be known *a priori* in order to reduce the number of unknown parameters in the inverse problem.

II. Ultrasonic scattering models for the estimation of QUS parameters

This section presents the four ultrasonic scattering models used in the present study to estimate the QUS parameters: the monodisperse sparse model (*model 1*, usually termed the fluid-filled sphere model), the polydisperse sparse model (*model 2*), the monodisperse concentrated SFM (*model 3*) and the polydisperse concentrated SFM (*model 4*). All four models consider ensembles of discrete fluid-filled spheres in a surrounding fluid medium.

We assume weak scattering contrast such that the differential backscattering cross section from a single fluid-filled sphere σ_b is given by [4]:

$$\sigma_b(k,r) = \frac{k^4 V_s^2 \gamma_z^2}{4\pi^2}\left(\frac{3}{2kr}j_1(2kr)\right)^2, \qquad (1)$$

where k is the wavenumber, r is the sphere radius, V_s is the sphere volume, j_1 is the spherical Bessel function of the first kind of order 1 and γ_z is the relative acoustic impedance difference between the scatterers and the surrounding tissue $\gamma_z = (z - z_0)/z_0$.

A. Monodisperse sparse model - Model 1

By considering an ensemble of identical discrete scatterers of radius a that are randomly and independently distributed, each scatterer equally and individually contributes to the backscattered power. It means that each scatterer scatters the incident waves unaffected by the presence of the other scatterers. The BSC is thus proportional to the average number of scatterers per unit volume n (also called the number density related to the volume fraction of scatterers ϕ and the scatterer volume V_s as n=ϕ/V_s) as follows:

$$\begin{aligned} BSC_{\text{sparse,mono}}(k) &= n\sigma_b(k,a) \\ &= n_z \frac{k^4 V_s^2}{4\pi^2}\left(\frac{3}{2ka}j_1(2ka)\right)^2. \end{aligned} \qquad (2)$$

With model 1, the two unknown parameters are the scatterer radius a^* and the acoustic concentration n_z^*.

B. Polydisperse sparse model - Model 2

When considering a polydisperse size distribution, *i.e.*, an ensemble of scatterers differing only in size with radius r, the BSC is given by:

$$\begin{aligned} BSC_{\text{sparse,poly}}(k) &= n\int_0^\infty \sigma_b(k,r)p(r)dr, \\ &= n_z\frac{4k^4}{9}\int_0^\infty \left(\frac{3}{2kr}j_1(2kr)\right)^2 r^6 p(r)dr, \end{aligned} \tag{3}$$

where p is the sphere radius probability distribution function (PDF). The acoustic concentration n_z is defined as $n_z = \frac{\phi\gamma_z^2}{(4/3)\pi\int_0^\infty p(r)r^3dr}$. The sphere radius distribution is assumed to be gamma (Γ) distributed with a PDF given by:

$$p_{(\zeta,\bar{a})}(r) = \frac{1}{\Gamma(\zeta+1)}\left(\frac{\zeta+1}{\bar{a}}\right)^{\zeta+1} r^\zeta e^{-(\zeta+1)r/\bar{a}}, \tag{4}$$

where $\bar{a}$ is the mean radius and ζ is the gamma width parameter (a large value of ζ corresponds to a narrow size distribution). In this paper, p will always be a gamma PDF and the subscript $(\zeta,\bar{a})$ will be omitted.

With model 2, the three unknown parameters are the mean scatterer radius $\bar{a}^*$, the gamma width factor ζ^* (or equivalently standard deviation SD_a^*=$\bar{a}^*/\sqrt{\zeta^*+1}$) and the acoustic concentration n_z^*.

C. Monodisperse concentrated Structure Factor Model (SFM) - Model 3

Models 1 and 2 are only valid if the medium has a low scatterer concentration. For a dense and monodisperse scattering medium, the presence of densely packed scattering sources introduces correlation between the phases of individually scattered waves, that can be modeled with the structure factor S [17]. When considering a concentrated medium with identical scatterers of radius a, the BSC using the monodisperse concentrated SFM is expressed as [15], [17]

$$BSC_{\text{SFM,mono}}(k) = n\sigma_b(k,a)S(k,a,\phi). \tag{5}$$

For an ensemble of identical hard (*i.e.*, non-deformable) spheres that are homogeneously distributed, the structure factor S can be analytically computed as established by Ashcroft (see Eqs. (3)-(5) in [19]). With model 3, the three unknown parameters are the radius a^*, the volume fraction ϕ^* and the relative acoustic impedance difference γ_z^*.

D. Polydisperse concentrated Structure Factor Model (SFM) - Model 4

When considering a polydisperse size distribution, with an ensemble of scatterers differing in size with radius r and scattering amplitudes $\Phi(k,r)$, the BSC using the polydisperse SFM is given by [11], [18] (referred as polydisperse model II in Ref. [11]):

$$\begin{aligned} &BSC_{\text{SFM,poly}}(k) = n\int_0^\infty |\Phi(k,r)|^2 p(r)\mathrm{d}r + \\ &n\int_0^\infty\int_0^\infty \Phi(k,r_1)\Phi(k,r_2)H_{12}(k)p(r_1)p(r_2)\mathrm{d}r_1\mathrm{d}r_2, \end{aligned} \tag{6}$$

where H_{12} is the partial structure function. The analytical expression of Eq. (6) can be obtained by considering fluid spheres with scattering amplitude $\Phi(k,r)$ derived from the fluid sphere form factor (as $|\Phi(k,r)|^2$=$\sigma_b(k,r)$) and by considering that the sphere radii follow a gamma PDF. With model 4, the four unknown parameters are the mean scatterer radius $\bar{a}^*$, the gamma width factor ζ^* (or equivalently standard deviation SD_a^*=$\bar{a}^*/\sqrt{\zeta^*+1}$), the volume fraction ϕ^* and the relative acoustic impedance difference γ_z^*.

Figure 1 shows examples of theoretical BSCs computed with model 4 for sets of fluid spheres with different mean radii $\bar{a}$, standard deviations SD_a, and volume fractions ϕ. The wavenumber in model 4 was computed as k=$2\pi f/c_0$, where c_0=1490 m.s^{-1} is the speed of sound in the surrounding medium. For all configurations studied, the acoustic impedance is identical γ_z=0.13. Changes in $\bar{a}$, SD_a or ϕ produce changes in the slope and amplitude of the BSCs. Specifically, increases in $\bar{a}$ or SD_a produce an increase in BSC amplitude at low frequencies (Figs. 1.a and 1.b). Whereas the BSC amplitude has a nonlinear relationship with the volume fraction of the scatterers (Fig. 1.c).

III. Material and Methods

A. Experiments

Three dense ensembles of cells with broad or narrow cell size distributions were considered in this study to investigate the effects of scatterer size distribution on QUS estimates. The BSCs measured on these dense ensembles of cells were obtained from experiments performed in Ref. [13]. Cell pellet fabrication, ultrasound acquisition and BSC measurements are described in details in Section Material and Methods of Ref. [13]. In summary, the cell pellets were created by centrifugation of colon adenocarcinoma (HT29) cells and thus consisted of densely packed cells with high cellular volume fractions around 73% [13]. This value of 73% is close to the maximum volume fraction of gamma-distributed hard spheres in random close packing and lower than the maximum volume fraction of log-normal-distributed hard spheres in random close packing (≈92%) [20]. Two cell pellets were treated with staurosporine, an inducer of apoptotic cell death, to obtain broad cell size distributions and one untreated cell pellet gave a narrower cell size distribution. Ultrasonic backscatter measurements were performed with a Vevo 770 high-frequency ultrasound system (Visualsonics Inc., Fujifilm, Toronto, Canada) with two oscillating single-element focused transducers with center frequencies 20 MHz and 28 MHz to cover a wide frequency range from 10 to 42 MHz. The BSCs are then compensated for the effects of attenuation by using attenuation values obtained by an insertion-loss broadband technique [13]. Examples of measured BSC_{meas} in the 10-42 MHz bandwidth are given in Fig. 2.

HT29 cell pellet biophantoms are an excellent experimental tool to test the performance of scattering models, since the large whole cells were identified to be the sources of scattering in the cell pellets [13]. So the consideration of an ensemble of polydisperse fluid spheres (with the sizes of the whole cells and with uniform acoustic properties) is sufficient to model the

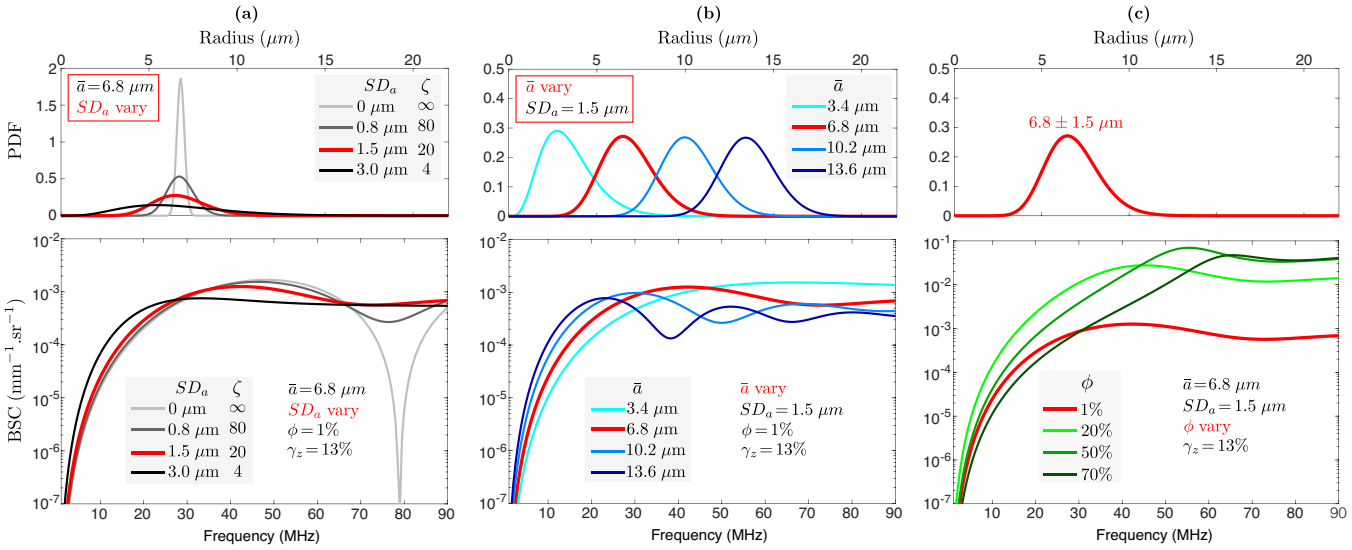

Fig. 1. Theoretical BSCs computed with the polydisperse concentration SFM (model 4) for different ensembles of fluid spheres with identical relative acoustic impedance difference γ_z=0.13 with (a) varying size standard deviations SD_a, (b) varying mean sphere radii $\bar{a}$ and (c) varying volume fractions ϕ.

BSCs from these HT29 cell pellets. The radius distribution of the large whole cells was fitted with a gamma PDF given in Eq. (4). Table I summarizes the mean radius $\bar{a}$ and the gamma width parameter ζ of the whole cells measured with a cell counter for the three cell pellets, as well as the corresponding standard deviation SD_a. Also given in Table I are the relative impedance contrast γ_z and cell volume fraction ϕ obtained by the optimization procedure developed in Ref. [13] to explain the behavior of the measured BSCs.

TABLE I
CHARACTERISTICS OF THE HT29 CELL PELLETS TREATED AND NON-TREATED WITH STAUROSPORINE

	Non-treated n°1	Treated n°2	Treated n°3
Mean radius $\bar{a}$ (μm)	6.8	7.2	5.7
Standard deviation SD_a (μm)	0.9	1.77	1.75
Gamma width parameter ζ	55.6	16.4	10.6
Impedance contrast γ_z	0.25	0.25	0.25
Volume fraction ϕ	0.73	0.73	0.73

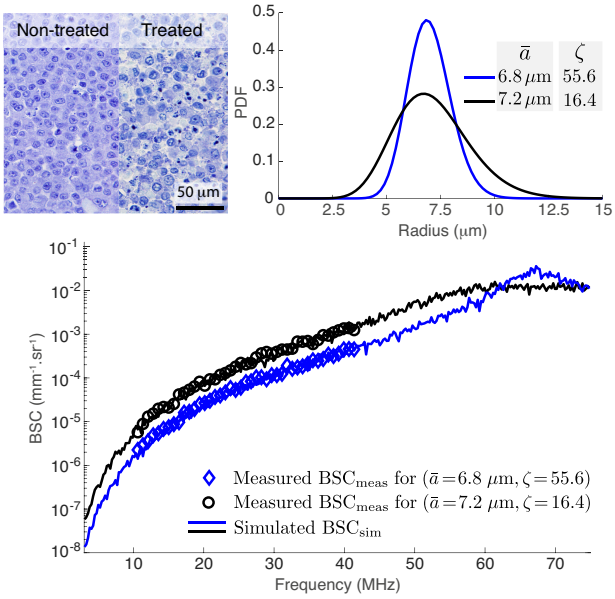

Fig. 2. (Top left) Examples of histological images of HT29 cell pellet biophantoms non-treated and treated with staurosporine. (Top right) Examples of whole cell-radius distribution for cells non-treated and treated with staurosporine. (Bottom) Corresponding measured BSC$_{meas}$ and simulated BSC$_{sim}$ by using γ_z=0.25 and ϕ=73%

B. Simulated BSC data

To study the effects of scatterer size distribution on QUS estimates, we perform inversions with controlled BSC data. These controlled BSC data consists in theoretical predictions of the BSCs (by using model 4) for which random noise was added to mimic experimental BSC noise. By abuse of language, these BSCs are called the simulated BSC data, denoted BSC_{sim}, in the remainder of the paper. The simulated data were computed as: $BSC_{\text{sim}}(k) = BSC_{\text{SFM,poly}}(k) \times$noise. The noise term was produced using a random number generator (with the routine *randn* in Matlab - The MathWorks, Inc., Natick, MA) which was a normal distribution of a mean of 1 and a standard deviation of 0.2.

First, ensembles of polydisperse fluid spheres were considered with mean radius $\bar{a}$=6.8 μm, gamma width parameters ζ=4, 20, 50 and 80 (corresponding to standard deviations of SD_a=3.0, 1.5, 1.0 and 0.8 μm) and volume fractions ϕ=1% and 20%. The relative acoustic impedance difference was chosen to be equal to γ_z =0.13 by considering impedance values of 1.48 MRayl for background and of 1.67 MRayl for scatterers [21]. Second, ensembles of dense polydisperse fluid spheres (ϕ=73%) were studied to mimic the experimental data for the

HT29 cell pellets treated and untreated with staurospaurine with the characteristics given in Table I. Example of simulated BSC_{sim} are given in Fig. 2.

C. Estimation of QUS parameters

The simulated or experimental BSC was fitted to a theoretical model (presented in section II) to estimate QUS parameters. Table II summarizes the estimated QUS parameters according to the scattering model used for the fitting procedure.

TABLE II
QUS ESTIMATES ACCORDING TO THE MODEL USED.

Model	Estimated QUS parameters
Model 1 - Monodisperse sparse	a^*, n_z^*
Model 2 - Polydisperse sparse	$\bar{a}^*$, SD^*, n_z^*
Model 3 - Monodisperse SFM	a^*, ϕ^*, γ_z^*
Model 4 - Polydisperse SFM	$\bar{a}^*$, SD^*, ϕ^*, γ_z^*

The optimization procedure to determine the QUS estimates consists in minimizing the relative mean error between the measured BSC_{meas} and the theoretical BSC_{theo}:

$$\mathcal{F} = \sum_j \| \frac{\text{BSC}_{\text{meas}}(k_j) - \text{BSC}_{\text{theo}}(k_j)}{\text{BSC}_{\text{meas}}(k_j)} \|^2 . \quad (7)$$

In the case of the sparse models 1 and 2, the fitting procedure was performed by using the routine *fminsearch* of MATLAB (The Mathworks Inc., Natick, MA), *i.e.* the Nelder-Mead simplex method. In the case of the concentrated models 3 and 4, the fitting procedure was performed by using the constrained minimization routine *fmincon* of MATLAB with the following constraint conditions: [$1 \leq a \leq 100\mu$m, $0.005 \leq \gamma_z \leq 0.4$ and $0 \leq \phi \leq 74\%$] for model 3, and [$1 \leq a \leq 100\mu$m, $1 \leq \zeta \leq 150$, $0.005 \leq \gamma_z \leq 0.4$ and $0 \leq \phi \leq 100\%$] for model 4. The *fmincon* routine was used mainly to avoid the unrealistic γ_z^* values that can occur with the *fminsearch* routine, as discussed later in section IV-D. Ten and twenty random initializations were used in our implementation for model 3 and model 4, respectively.

When using the sparse models 1 and 2, the volume fraction and the acoustic parameters cannot be estimated separately, such that the QUS parameters are the mean scatterer radius $\bar{a}^*$ and the acoustic concentration n_z^*. In order to compare the QUS estimates of the four models, n_z^* was also calculated when using models 3 and 4:

$$n_z^* = \frac{\phi^* \gamma_z^{*2}}{E[V_s]} = \frac{\phi^* \gamma_z^{*2}}{\frac{(\zeta+3)(\zeta+2)}{(\zeta+1)^2} \frac{4\pi \bar{a}^{*3}}{3}}. \quad (8)$$

Note that, when using model 3, ζ tends towards ∞ and the value of $(\zeta+3)(\zeta+2)/(\zeta+1)^2$ in Eq. (8) tends towards 1.

The QUS parameters were estimated at different center frequencies f_0 by fitting the measured or simulated BSC in the frequency bandwidth $[f_{\text{min}} - f_{\text{max}}] = [0.5 f_0 - 1.5 f_0]$, *i.e.*, corresponding to transducers with 100% usable bandwidth.

IV. RESULTS AND DISCUSSION

A. QUS estimates from simulations with fluid spheres for sparse media (ϕ=1%)

Figure 3 gives the radius $\bar{a}^*$ and the acoustic concentration n_z^* estimated by the four scattering models when considering an ensemble of fluid spheres sparsely distributed at ϕ=1% and ζ=4, 20, 50 and 80.

Model 1, that does not take into account the polydispersity, estimates correctly the radius and the acoustic concentration for the narrower size distributions (ζ=50 and 80) for frequencies above 16 MHz. In these cases, the relative errors are less than 10% for $f_0 \geq$16 MHz. However, when the size distribution becomes wider with ζ=5 and 20, the assumption of monodisperse media breaks down, so that model 1 overestimates the actual scatterer radius and underestimate the acoustic concentration, even more so for ζ=4 (*i.e.*, the largest SD_a). The scatterer size estimates are larger than the reality, because the increase in scatterer size variance modifies the BSC slope that is more influenced by the largest scatterers. Since larger scatterer radii have the effect to rise the BSC amplitude, model 1 underestimates the acoustic concentration to compensate for this effect. Note that for the highly polydisperse media, model 1 does not provide good fits to the data with goodness-of-fit statistic $r^2 < 0$ for $f_0 \geq$ 31 MHz at ζ=4 and for $f_0 \geq$49 MHz at ζ=20.

One can notice that both monodisperse models 1 and 3 gave similar QUS parameters for high frequency values $f_0 >$26 MHz (corresponding to $ka >$0.75) whatever the studied gamma width parameters. However, at low frequencies, the monodisperse concentrated model 3 converge more slowly towards actual values when compared to the monodisperse sparse model 1. Indeed, for the polydispersities ζ= 20, 50 and 80 at lower frequencies $f_0 <$26 MHz, scatterer sizes are largely overestimated, acoustic concentrations are underestimated (as shown in Fig. 3), and volume fractions are overestimated for $f_0 <$26 MHz (data not shown). This is due to the difficulty to estimate simultaneously three parameters a, ϕ and γ_z with model 3 for sparse media, as discussed previously in [15]. Briefly, model 3 uses the frequency-dependent BSC behavior, defined by the product $\sigma_b(k,a)S(k,a,\phi)$, to estimate the parameters a and ϕ. However, for sparse media, the structure factor is approximately equal to 1 at all frequencies and does not modify the BSC slope. That is why model 3 encounters difficulty to estimate the parameters a and ϕ, and cannot provide robust estimation of QUS parameters at low frequencies in the case of sparse media.

Models 2 and 4 considering polydisperse media show different results. The mean scatterer radii estimated by the sparse model 2 match well the actual mean radius for the highly polydisperse medias ζ=4 and 20 (see QUS estimates in Fig. 3 from 22 MHz to 50 MHz for ζ=4, and from 26 MHz to 50 MHz for ζ=20). But for the narrower size distributions ζ=50 and 80, the polydisperse sparse model 2 is less efficient than the monodisperse sparse model 1. This limitation is caused by the fact that both mean radius and size variance

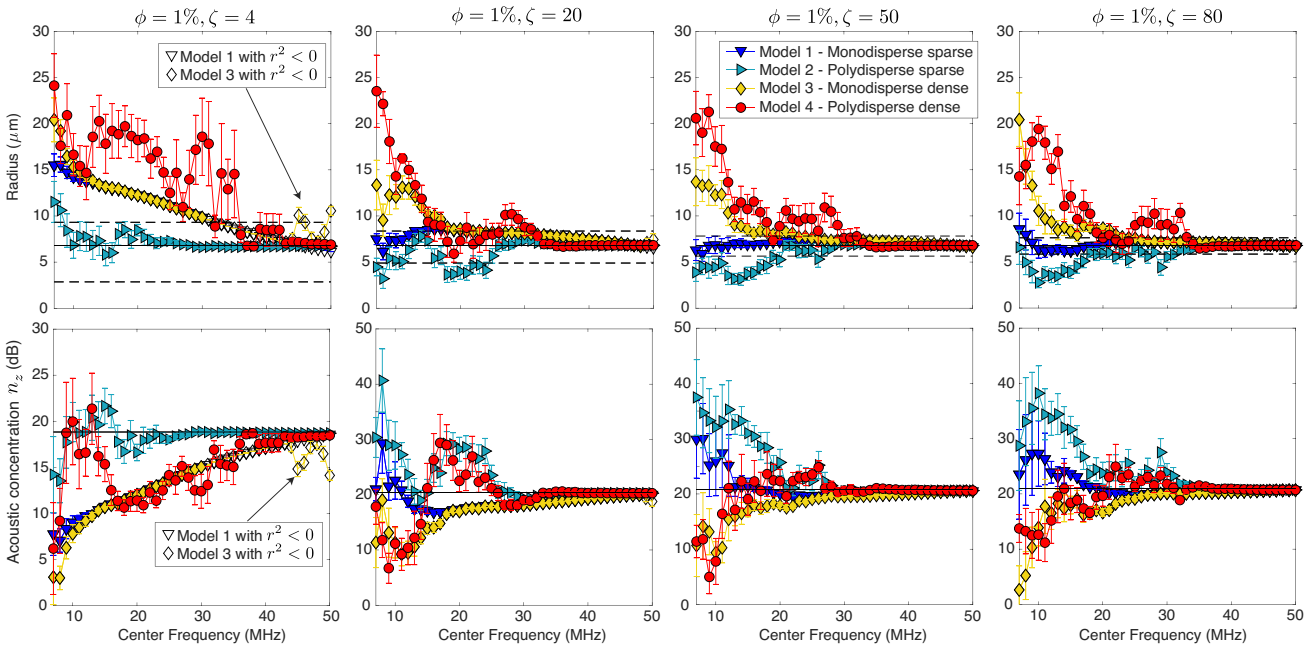

Fig. 3. Scatterer radii $\bar{a}^*$ and acoustic concentration n_z^* estimated by inversion procedure. Results are obtained from the simulated BSC_{sim} for an ensemble of fluid spheres at ϕ=1%, $\bar{a}$=6.8 μm, ζ=4, 20, 50 and 80 (corresponding to SD_a=3.0, 1.5, 1.0 and 0.8 μm). The black solid lines represent the expected values. In the top panel, the horizontal dashed lines indicate the lower and upper bounds of scatterer radii in the actual radius distribution (full width at half maximum). The empty symbols represent the inversion results for which models 1 and 3 do not provide good fits to the data (r^2 <0).

influence the BSC slope. Model 2 uses the slope of the BSC to jointly estimate the radius and the polydispersity, which is less efficient than model 1, which only estimates radius by using the BSC slope. Similarly, model 4 is less efficient than model 2 in estimating QUS parameters. All QUS parameters ($\bar{a}^*$, SD_a^*, ϕ^* and γ_z^*) estimated by model 4 are very unstable for f_0 <40 MHz. The cause of this problem is the number of parameters estimated with model 4. An inversion performed to estimate four parameters is more unstable than an inversion performed to estimate three parameters. Therefore, the estimations of $\bar{a}^*$, SD_a^*, n_z^* is less reliable with the polydisperse concentrated model 4 than with the polydisperse sparse model 2. Model 4 only provides satisfactory QUS estimates for f_0>42 MHz.

B. QUS estimates from simulations with fluid spheres for moderately dense media (ϕ=20%)

The estimated values of a^* and n_z^* are presented in Fig. 4 considering an ensemble of fluid spheres for ϕ=20% and different gamma width factors ζ=4, 20, 50 and 80. Figure 5 gives some examples of SD_a^*=$\bar{a}^*/\sqrt{\zeta^*+1}$ estimated by the polydisperse models 2 and 4.

For the polydispersities ζ=20, 50 and 80, the sparse models 1 and 2 gave similar QUS estimates a^* and n_z^*, since the standard deviations SD_a^* estimated by model 2 tend towards the zero value (Fig. 5(b)). For frequencies less than 40 MHz, the sparse models 1 and 2 underestimate the mean radius and overestimate the acoustic concentration for the polydispersities ζ= 20, 50 and 80, as expected for concentrated media [15]. *A contrario*, for frequencies above 40 MHz, both models 1 and 2 estimate correctly the QUS parameters, which constitutes surprising results for models not adapted to concentrated media. To interpret these results, it is useful to pay attention to the behavior of the structure factors for different ζ values given in Fig. 6(a), since the structure factor gives the frequencies that are influenced by the correlation position of the scatterers. One can observe that the structure factor oscillates around the value of 1 with a deviation of less than 0.2 for f_0>40 MHz, meaning that the correlation position effect is weaker for these frequencies. Moreover, the frequencies f_0>40 MHz are sufficiently high to obtain accurate measurements of scatterer sizes, since the product ka is greater than 1.1 [22]. The mean scatterer's size is thus the principal factor determining the frequency dependence of the BSC for frequencies above 40 MHz, so models 1 and 2 perform well in estimating the QUS parameters. For f_0<40 MHz, the structure factors are much smaller than 1, as shown in Fig. 6(a), which means that destructive interferences occur. The sparse models 1 and 2 do not account for these interference effects and thus cannot correctly estimate the QUS parameters.

For the highly polydisperse medium ζ=4, the polydisperse sparse model 2 provides better QUS estimates a^* and n_z^* than the concentrated model 4 (Fig. 4), especially for 30≤f_0≤40 MHz, since the structure factor is approximately equal to 1 for ζ=4 for f_0>30 MHz (Fig. 6(a)). However, model 2 underestimates the standard deviation SD_a. The monodisperse sparse model 1 overestimates the mean scatterer size and does not provide good fits to the data with goodness-of-fit statistic r^2 <0 for f_0 ≥38 MHz (just like model 3, since monodisperse models are not suitable for this highly polydisperse medium).

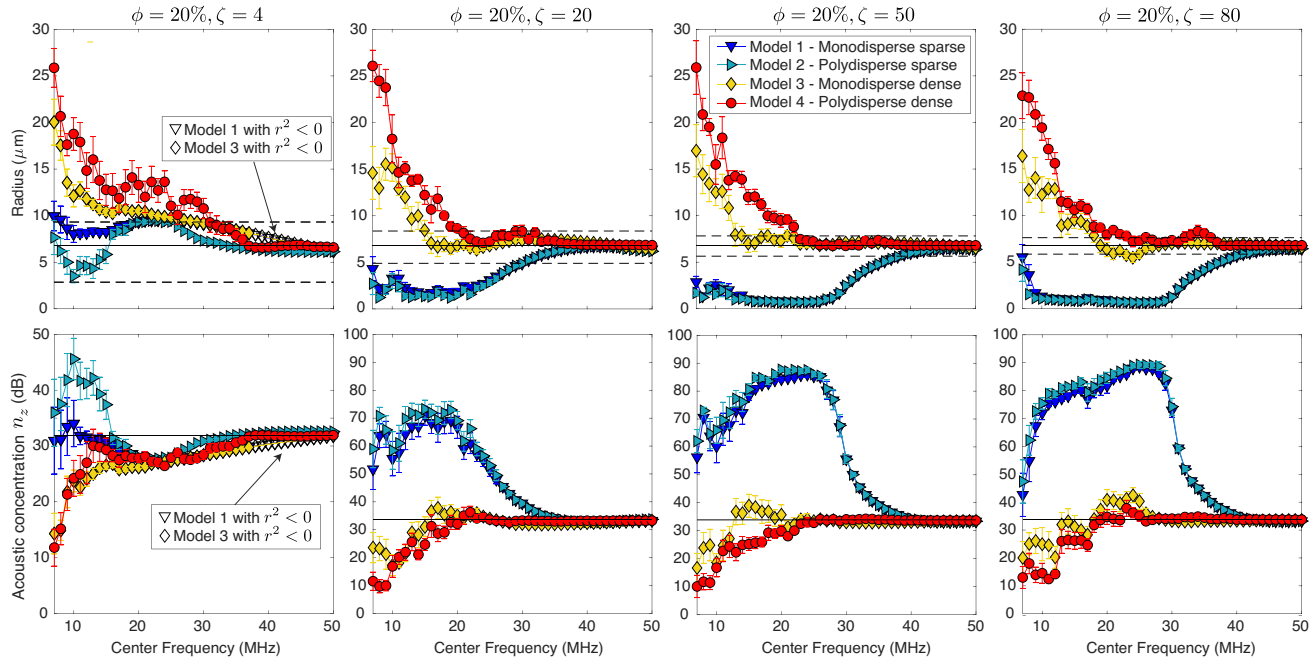

Fig. 4. Scatterer radii $\bar{a}^*$ and acoustic concentration n_z^* estimated by inversion procedure. Results are obtained from the simulated BSC_{sim} for an ensemble of fluid spheres at ϕ=20%, $\bar{a}$=6.8 μm, ζ=4, 20, 50 and 80 (corresponding to SD_a=3.0, 1.5, 1.0 and 0.8 μm).

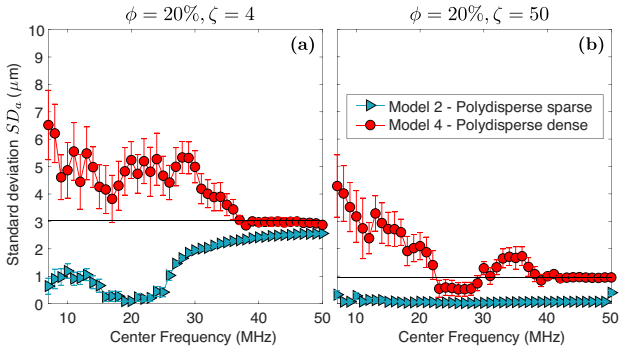

Fig. 5. Standard deviation SD_a^* estimated by inversion procedure. Results are obtained from the simulated BSC_{sim} for fluid spheres with (a) ϕ=20% and ζ=4 and (b) ϕ=20% and ζ=50. The black solid lines represent the expected values.

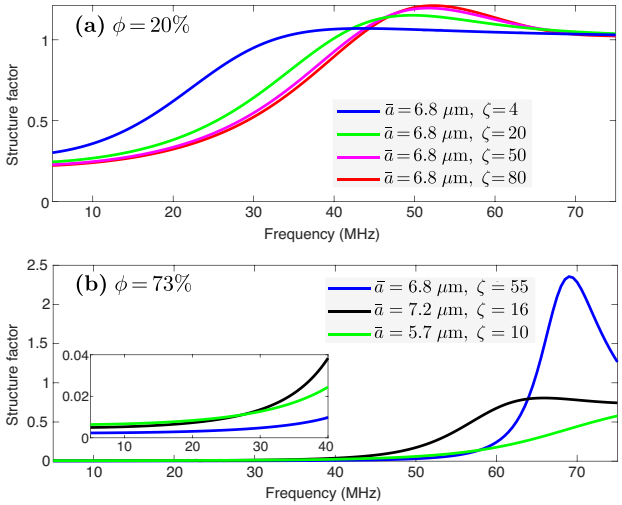

Fig. 6. Structure factors $S(k)$ as a function of frequency for ensembles of fluid spheres (a) for ϕ=20% and (b) for ϕ=73%.

However, for f_0<14 MHz, model 1 matches the expected values better than the other models. It is due to the fact that (by chance) model 1 with [a=8 μm and n_z=31.97 dB] and model 4 with [$\bar{a}$=6.8 μm, ζ=4, γ_z=0.13 and ϕ=20%] produce the same BSC at low frequencies f_c<20 MHz (Fig. 7).

The concentrated models 3 and 4 provide mean radii and acoustic concentrations closer to the expected values for a wide range of frequencies, when compared to the sparse models 1 and 2. As the frequency f_0 decreased, both models 3 and 4 give scatterer radius estimates that fell outside the range of underlying scatterer sizes. Overall, the QUS estimates a^* and n_z^* obtained with models 3 and 4 are in good agreement for moderate to high f_0 values. However, model 3 outperforms model 4 for moderate f_0 values: model 4 fails in estimating the mean scatterer size for $f_0 \leq 23$ MHz, against $f_0 \leq 15$ MHz for model 3 (see QUS estimates in Fig. 4 for ζ=20 and 50). Using model 4, all three parameters $\bar{a}$, ζ, and ϕ can influence the frequency dependence of the BSC, and therefore, it is difficult to separate their effects.

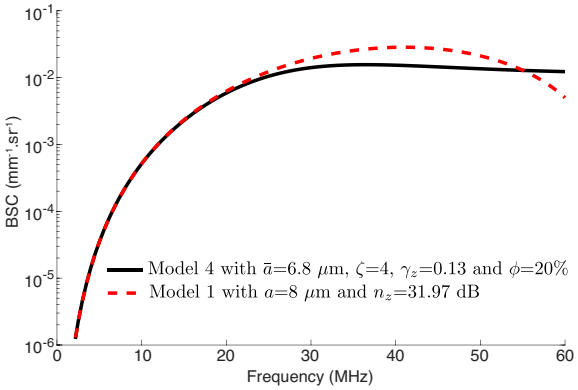

Fig. 7. Comparison of two theoretical BSCs by using model 1 with [a=8 μm and n_z=31.97 dB] and model 4 with [$\bar{a}$=6.8 μm, ζ=4, γ_z=0.13 and ϕ=20%].

C. QUS estimates from simulations and experiments for concentrated media (ϕ=73%)

The parameters a^* and n_z^* estimated by the four scattering models are presented in Fig. 8 for concentrated media (ϕ=73%). Results are given for the simulated BSC_{sim} (solid lines) and for the measured BSC_{meas} obtained from the cell pellet biophantoms (symbols). Also represented in Fig. 8 are the parameters SD_a^* estimated by the polydisperse models 2 and 4, and ϕ^* and γ_z^* estimated by the concentrated models 3 and 4.

The sparse models 1 and 2 underestimate the mean radius and overestimate the acoustic concentration for moderate to high f_0 values, as expected for concentrated media. One can notice that the mean radius estimated with model 1 fell within the actual size range for low f_0 values in the case of the broad cell size distribution (for f_0 <12 MHz with ζ=16.4 and for f_0 <27 MHz with ζ=10.6). This result was unexpected since the structure factors are very different for the value of 1, as shown in Fig. 6(b). In this scattering regime $k\bar{a}$ <0.7, the structure factor obtained at ϕ=73% causes a large decrease in the BSC amplitude and a slight increase in the BSC spectral slope. Whereas the increase in scatterer size distribution has the effect to increase the BSC amplitude and to decrease the BSC spectral slope. These combined effects seem to cancel, so that model 1 produces quite satisfactory mean scatterer radii for low f_0 values.

Model 3 provides a^* and n_z^* estimates that match well the actual parameters for the narrow size distribution ($\bar{a}$=6.8 μm, ζ=55.6) and for high f_0 values (f_0>35 MHz corresponding to $k\bar{a}\approx$1), as expected. For broad scatterer size distribution, model 3 produces QUS estimates that are most of the time outside the range of expected values. The volume fraction ϕ^* is largely underestimated whatever the considered f_0. The estimated radius a^* and acoustic concentration n_z^* are unstable: a^* has the tendency to decrease (and n_z^* to increase) as f_0 increases. Whereas, model 4 provides satisfactory QUS estimates for the three considered cases for high f_0 values (f_0>40 MHz).

Overall, the simulated and experimental results yielded QUS estimates that fell within the same range of values when using the four scattering models. Nevertheless, it can be observed in Fig. 2 that the QUS estimates obtained by simulations and experiments may differ even if both simulated and measured BSC follow the same trends (Fig. 2). When using model 4, the 28 MHz probe is more efficient to estimate the parameters a^* and n_z^*, when compared to the 20 MHz probe.

D. Choice of the optimization procedure

In the present study, the QUS parameters estimated with the concentrated SFM models 3 and 4 are estimated by using the constrained minimization routine *fmincon*. One may question the choice of an optimization method with or without constraints. As an example, Fig. 8(d) compares the QUS parameters estimated by models 3 and 4 by using the routines *fmincon* (optimization with constraints) and *fminsearch* (optimization without constraint) for a given example of [$\bar{a}$=7.2 μm, ζ=16.4, γ_z=25%, ϕ=73%]. When using model 4, both routines *fmincon* and *fminsearch* give similar mean scatterer radius $\bar{a}^*$ and acoustic concentration n_z^*. When using model 3, the estimates a^* and n_z^* may differ depending on the routine used. We observed that the *fminsearch* routine provides the global minimum (data not shown), but could result in unrealistic values with a large overestimation of γ_z^* (>40%) (Fig. 8d). That is why the *fmincon* routine was used to avoid the unrealistic γ_z^* values that can occur with the *fminsearch* routine. Note that a systematic comparison between the routines *fmincon* and *fminsearch* was previously performed by Muleki-Seya et al. [25] on *ex vivo* tumor models using model 3, and these unrealistic values of QUS parameters were also found. As it can be observed in Fig. 8d, no improvement on the QUS estimates was observed by using the *fminsearch* routine, as the behaviors of the QUS estimates versus frequency curves are still very unstable when considering model 3. (Similar results were obtained with the other scatterer size distributions - data not shown.)

In this article, the cost function uses the relative mean squared error of the BSCs to provide the QUS parameters. However, it is important to recall that the QUS parameters can be affected by the choice of cost functions [8] [15]. In a previous study, Franceschini et al. [15] compared two optimization strategies that consist of minimizing either the relative mean squared error (Eq. (7) in the present study) or the absolute mean squared error (Eq. (14) in Ref. [15]) for studying media with scatterer volume fractions ranging from 0.6% and 30%. The relative mean squared error mainly weights all the frequencies equally in the frequency bandwidth studied, whereas the absolute mean squared error penalizes large absolute difference at high frequencies more strongly. Both optimization strategies in [15] were used to estimate QUS parameters by fitting the measured BSC to a theoretical BSC by investigating several scattering models: the sparse spherical Gaussian model, the sparse fluid-filled sphere model (model 1 here) and the monodisperse structure factor model (model

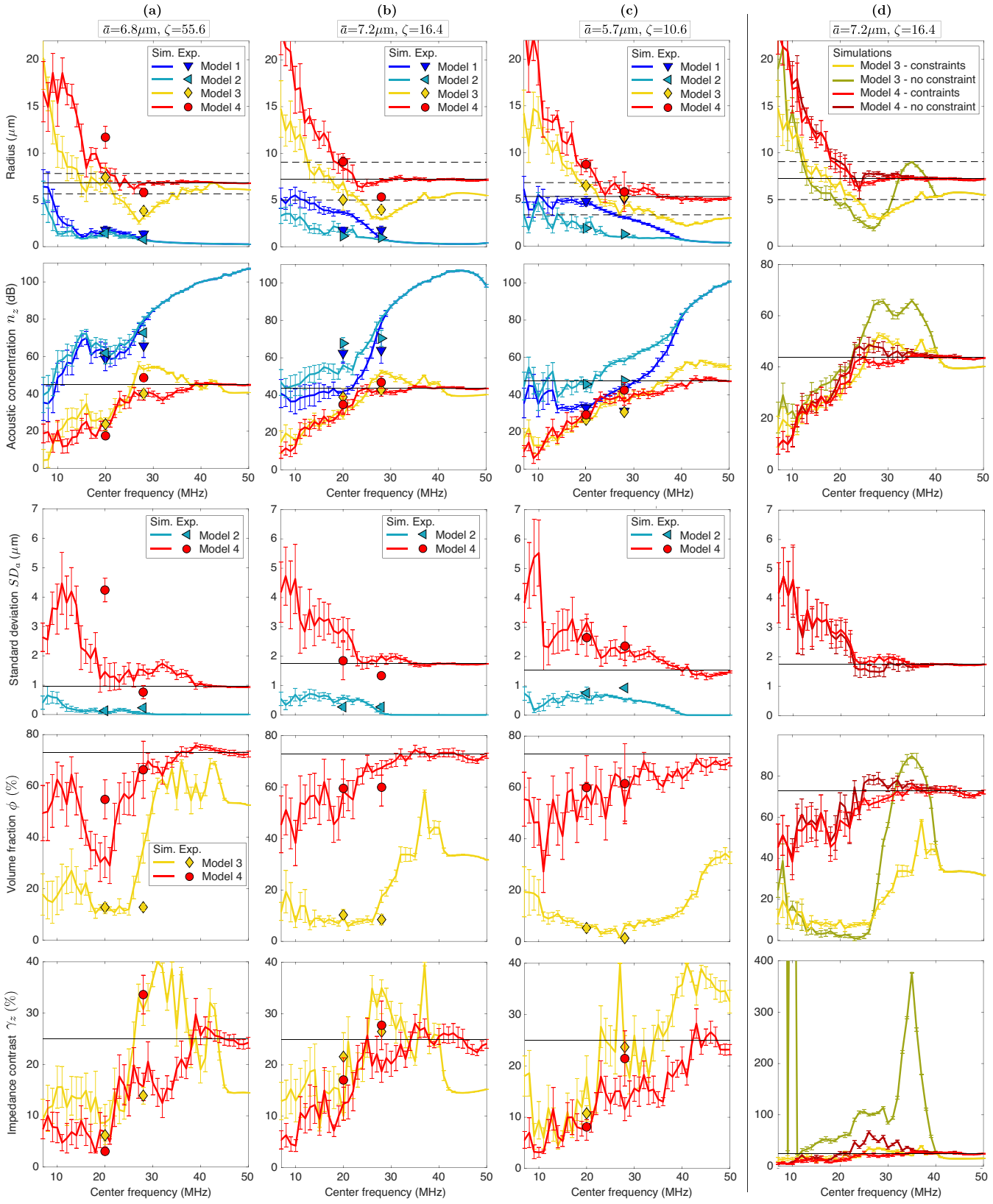

Fig. 8. (a), (b) and (c) Scatterer radii $\bar{a}^*$, acoustic concentration n_z^*, volume fraction ϕ^* and impedance contrast γ_z^* estimated by inversion procedure in the case of concentrated media (ϕ=73%). Results are obtained from the simulated BSC_{sim} (solid lines) and from the measured BSC_{meas} (symbols) for three different couples of parameters ($\bar{a}$, ζ). (d) Comparisons of QUS parameters by using optimization procedures with and without constraints obtained from the simulated BSC_{sim} for [$\bar{a}$=7.2 μm, ζ=16.4].

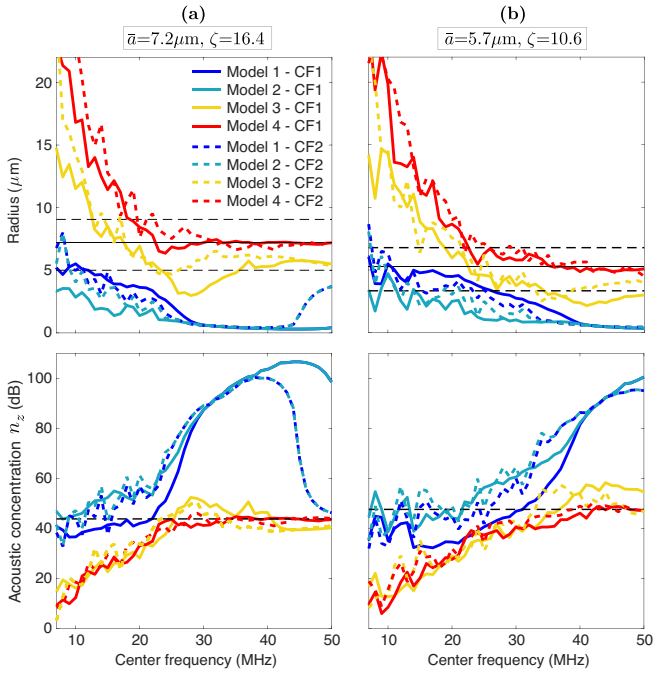

Fig. 9. Comparisons of the estimates of $\bar{a}^*$ and n_z^* by using the relative mean squared error (denoted CF1) or by using the absolute mean squared error (denoted CF2). The cost function CF1 is given in Eq. (7) and the cost function CF2 is given in Eq. (14) in Ref. [15]. Results are obtained from the simulated BSC_{sim} from two scattering configurations [$\bar{a}$=7.2 μm, ζ=16.4, γ_z=25%, ϕ=73%] and [$\bar{a}$=5.7 μm, ζ=10.6, γ_z=25%, ϕ=73%].

3 here). As it can be observed in Fig. 7 of Ref. [15], the two cost functions can yield different estimates of a^* and n_z^*: estimates with model 3 differ mainly for lower volume fractions ($\phi \leq 5\%$), while estimates with sparse model 1 differ for higher volume fractions ($\phi \geq 12\%$). In a similar way to that was done in Ref. [15], Fig. 9 compares the estimates of a^* and n_z^* by using the relative mean squared error or the absolute mean squared error for two concentrated scattering configurations with ϕ=73%. Whatever the cost functions used, model 3 underestimates the scatterer radius at high frequencies, but the estimates are generally closer to the values expected with the cost function using the mean-square absolute error. It is interesting to observe that the radii estimated with model 4 are similar for both cost functions at high frequencies $f_c \geq 30$ MHz, whereas they can differ strongly with model 3 (e.g., for $\bar{a}$=5.7 μm and ζ=10.6 at $36 \leq f_c \leq 50$ MHz) and with models 1 and 2 (e.g., for $\bar{a}$=7.2 μm and ζ=16 at $f_c \geq 44$ MHz). This suggests that the QUS parameters vary more strongly with the two cost functions considered when the scattering models are not adapted.

E. Choice of the simulation methods

In our previous numerical studies [15], [16], the simulated BSC_{sim} was obtained using a semi-analytical approach. This approach involved a two-step process. Firstly, a random distribution of cells with non-overlapping positions was generated. Secondly, the BSC_{sim} was computed by summing the contribution of each scatterer while considering the associated phase terms related to their locations (see Eq. (9) in Ref. [15]). The different realizations of the medium allowed us to mimic the experimental noise of the BSC. This semi-analytical approach has the advantage to take into account different scatterer sizes, shapes and acoustic properties. However, it is generally limited to a moderate volume fraction (up to 30%). To overcome this limitation, we opted for an alternative approach in the current study by introducing noise into the theoretical BSC prediction obtained with model 4. This allowed us to reach a higher volume fraction ϕ=73%. It is interesting to note that the QUS estimates obtained in the present numerical studies show a remarkable similarity with the preliminary results based on the semi-analytical approach [16] (at ϕ=1% and 20%). The agreement of the results obtained by the alternative method presented here further strengthens its validity. By adopting this alternative simulation method, we were able to address the limitations associated with the semi-analytical approach, allowing for the investigation of higher volume fractions and broadening the scope of our study.

Finally, it is worth noting that the results in the present study are not universal and are most likely affected by the chosen optimization procedure (as discussed earlier in IV-D), but also by the chosen scattering configuration (*i.e.*, the chosen $\bar{a}$, ζ and ϕ) and measurement noise. Complementary simulations were conducted to study the influence of the noise levels on QUS estimates. Figure 10 shows examples of QUS estimates obtained from the simulated scattering configuration [$\bar{a}$=5.7 μm, ζ=10.6, γ_z=25%, ϕ=73%] with increasing noise levels using different standard deviations of 0.1, 0.2 and 0.3 for the random noise term. As expected, noise level has an impact on the behavior of QUS estimates. Overall, the standard deviation of the estimates increases with measurement noise. One can observe that model 4, which is the most adapted for this scattering configuration, converges more slowly towards the actual radii as the noise level increases. Noise reduction in BSC experiments is therefore of major interest. Several methods have been proposed in the literature, such as the increase of the number of independent data acquired using different angles of incidence under the assumption of isotropic scattering [23], or signal-processing techniques such as multitaper or Welch's method [24].

F. Choice of scattering models & Interpretation of QUS estimates for soft tissues

Previous works studied the effects of scatterer size distribution and/or frequency range on the scatterer size estimates when considering sparse media [5]–[8]. The work presented here complement these earlier works by focusing on moderately and highly concentrated media with gamma size distribution. Not surprisingly, models 1, 2 and 3 cannot provide physically meaningful estimates when the scattering media are polydisperse and dense, as shown in Fig.8. However, of particular interest are the results obtained with the moderately concentrated media (ϕ=20%) shown in Fig. 4. All the four models were able to correctly estimate the a^* and n_z^* at high

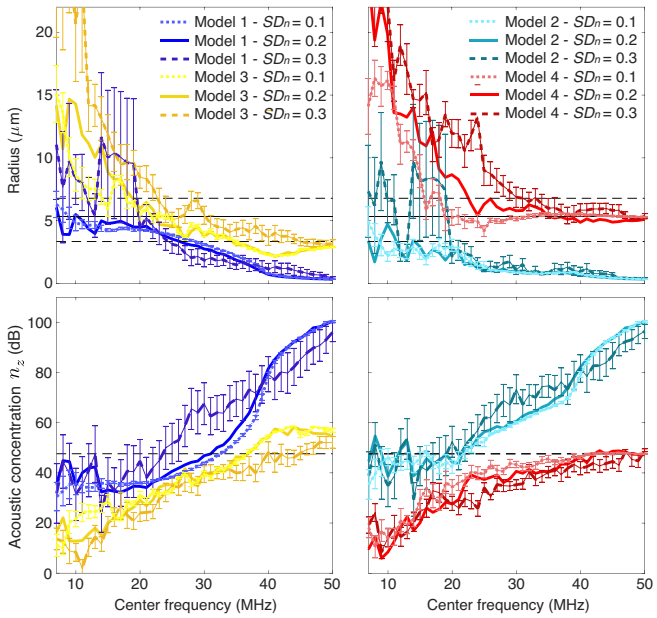

Fig. 10. Comparisons of the estimates of $\bar{a}^*$ and n_z^* for different levels of noise. The noise term used for the simulated BSC_{sim} had a normal distribution of a mean of 1 and a standard deviation SD_n of 0.1, 0.2 or 0.3. Standard deviations of QUS estimates are only presented for SD_n=0.1 and SD_n=0.3. The reader can refer to Fig. 8 for the results of SD_n=0.2. Results are obtained from the simulated scattering configuration [$\bar{a}$=5.7 μm, ζ=10.6, γ_z=25%, ϕ=73%].

frequencies (f_0>40 MHz), mainly because the interference effects caused by spatial correlations between scatterers are weaker for these frequencies at ϕ=20% (as already discussed in subsection IV-B). At sufficiently high frequencies, the structure factor oscillates around the value of 1, such that the correlation position effects can be neglected and sparse models can be efficient. In the present scattering configurations, the frequencies for which coherent scattering can be neglected are very high: more than 40 MHz at ϕ=20% and more than 80 MHz at ϕ=73% (Fig. 6).

The results presented here demonstrate that the scatterer size estimated by the monodisperse model 3 fail to represent actual tissue microstructure for polydisperse media, as expected. When using model 3, the most important biases in QUS estimates were obtained for the highly concentrated media ϕ=73%: a^* is overestimated at low frequencies and underestimated at high frequencies, and ϕ^* is underestimated at all frequencies. The wider the size distribution, the larger the radius errors for frequencies more than 25 MHz, as it can be observed in Fig. 8. In light of these results, the polydispersity in hepatocyte size explain why contradictory results have been found by using model 3 and model 4 in liver tissues: a^*=5.3 μm using model 3 in canine liver at 25 MHz (close to nuclear size) [25], against $\bar{a}^*\approx$14 μm using model 4 in rabbit liver or in human liver at 30 MHz (close to whole cell size) [26] [27]. (Note that the hepatocytes in canine livers in Ref. [25] present a wide distribution of the whole cell size: a=16.2$\pm$2.6 μm corresponding to ζ=38.) As it is more likely that the whole cells are the dominant sources of scattering in normal liver [26] [27], our results obtained for dense and polydisperse media in Fig. 8 may explain why the size of whole hepatocytes was underestimated in [25].

Contradictory results were also obtained with model 3 in *ex vivo* tumor models. The scatterer size estimates from model 3 were hypothesized to represent the whole cells in HT29 tumors at 30 MHz [25], as opposed to nuclei in 4T1, JC, LMTK and MAT tumors at 40 MHz [28]. Further studies need to be conducted in light of model 4 (or even other more elaborate modeling) to determine the actual sources responsible for scattering, which always remain a challenging question in the field of QUS.

Model 4 may provide a useful scattering model to progress in the understanding of the scattering sources in soft tissues for sufficiently high frequencies (f_0 >38 MHz corresponding to $k\bar{a}$ value more than 1). This need of using high frequencies obviously limits the applications to fundamental research studies for the understanding of scattering from *ex vivo* soft tissues and to clinical research studies on *in vivo* superficial tissues (e.g., skin, eye, blood vessel). The simulation results demonstrate that model 4 converges towards precise QUS estimates at sufficiently high frequencies. However, further studies need to be conducted on controlled experiments (*i.e.* cellular biophantoms, *ex vivo* tumors) to confirm these trends. In particular, stable QUS estimates with model 4 at different frequencies f_0 may help to be more confident about the physical meaning of the parameters. The effects related to mixtures of different scatterer types (e.g., tumor cell structures together with blood microvessels and/or fibrotic tissues implying different acoustic impedance properties and different size ranges) on the QUS estimates should also be investigated.

V. Conclusion

Four scattering models were assessed to study the effects of scatterer polydispersity and volume fraction on QUS estimates, namely scatterer size and acoustic concentration. Our findings reveal that the choice of scattering model has a significant impact on the accuracy of the QUS estimates. The effectiveness of a scattering model in determining QUS parameters is obviously closely linked to its ability to model the scattering medium. For sparse media, models 1 and 2 proved to be the most suitable options due to their ability to estimate a reduced number of parameters. For moderately dense media, model 4 gave promising results for high polydispersity values, while model 3 proved effective for lower polydispersity values. For dense media, model 4 proved the most accurate for quantifying QUS estimates at sufficiently high frequencies. However, since no *a priori* information can be used to determine whether a scattering medium is sparse, moderately dense or dense, the choice of scattering model is therefore not straightforward. In blind estimation of QUS parameters, the polydisperse concentrated model 4 can be recommended, provided it could be used at high enough frequencies.

This work provides valuable insights into the effects of size polydispersity and dense media on spectral-based QUS

techniques. By deepening further our understanding of these factors, we can enhance the interpretation and application of QUS techniques for diagnostic ultrasound in a wide range of clinical applications: disease assessment, tumor detection or treatment monitoring.

REFERENCES

[1] M. Oelze and J. Mamou, "Review of quantitative ultrasound: envelope statistics and backscatter coefficient imaging and contributions to diagnostic ultrasound," IEEE Trans. Ultrason. Ferroelect. Freq. Control **63**(2), 336–351 (2016).

[2] F. L. Lizzi, M. Greenebaum, E. J. Feleppa, and M. Elbaum, "Theoretical framework for spectrum analysis in ultrasonic tissue characterization," J. Acoust. Soc. Am. **73**(4), 1366–1373 (1983).

[3] M. L. Oelze and W. D. O'Brien, "Application of three scattering models to characterization of of solid tumors in mice," Ultrason. Imaging **28**(2), 83–96 (2006).

[4] M. F. Insana, R. F. Wagner, D. G. Brown, and T. J. Hall, "Describing small-scale structure in random media using pulse-echo ultrasound," J. Acoust. Soc. Amer. **87**(1), 179–192 (1990).

[5] V. Roberjot, S. L. Bridal, P. Laugier, and G. Berger, "Absolute backscatter coefficient over a wide range of frequencies in a tissue mimicking phantom containing two populations of scatterers," IEEE Trans. Ultrason. Ferroelectr. Freq. Control **43**(5), 970–978 (1996).

[6] J. Mamou, M. L. Oelze, W. D. O'Brien Jr., and J. F. Zachary, "Identifying ultrasonic scattering sites from three-dimensional impedance maps," J. Acoust. Soc. Am. **117**(1), 413–423 (2005).

[7] R. Lavarello and M. Oelze, "Quantitative ultrasound estimates from populations of scatterers with continuous size distribution," IEEE Trans. Ultras. Ferroelectr. Freq. Control. **58**(4), 744–753 (2011).

[8] R. Lavarello and M. Oelze, "Quantitative ultrasound estimates from populations of scatterers with continuous size distribution: Effects of the size estimator algorithm," IEEE Trans. ultras. Ferroelectr. Freq. Control. **59**(9), 2066–2076 (2012).

[9] E. P. Nordberg and T. J. Hall, "Effective scatterer diameter estimates for broad scatterer size distributions," Ultrason. Imaging **37**(1), 3–21 (2015).

[10] N. Jafarpisheh, I. M. Rosado-Mendez, T. J. Hall, and H. Rivaz, "Estimation of the scatterer size distributions in quantitative ultrasound using constrained optimization," 2021 IEEE International Ultrasonics Symposium (IUS), China (11-16 September, 2021), pp. 1–4.

[11] A. Han and W. D. O'Brien, "Structure function for high concentration biophantoms of polydisperse scatterer sizes," IEEE Trans. Ultrason. Ferroelectr. Freq. Control **62**(2), 303–318 (2015).

[12] M. Vlad, R. K. Saha, N. M. Alajez, S. Ranieri, G. J. Czarnota, and M. C. Kolios, "An increase in cellular size variance contributes to the increase in ultrasound backscatter during cell death," Ultrasound Med. Biol. **36**(9), 1546–1558 (2010).

[13] E. Franceschini, L. Balasse, S. Roffino, and B. Guillet, "Probe the cellular size distribution from cell samples undergoing cell death," Ultrasound Med. Biol. **45**(7), 1787–1798 (2019).

[14] R. de Monchy, J. Rouyer, F. Destrempes, B. Chayer, G. Cloutier, and E. Franceschini, "Estimation of polydispersity in aggregating red blood cells by quantitative ultrasound backscatter analysis," J. Acoust. Soc. Am. **143**(4), 2207–2216 (2018).

[15] E. Franceschini, R. de Monchy, and J. Mamou, "Quantitative characterization of tissue microstructure in concentrated cell pellet biophantoms based on the structure factor model," IEEE Trans. Ultras. Ferroelectr. Freq. Control. **63**(9), 1321–1334 (2016).

[16] O. Lombard, M. Audenay, and E. Franceschini, "Effects of polydispersity and high scatterer concentration on quantitative ultrasound estimates," 2022 IEEE International Ultrasonics Symposium (IUS), Venice, Italy (10-13 October, 2022), pp. 1–4

[17] V. Twersky, "Low-frequency scattering by correlated distributions of randomly oriented particules," J. Acoust. Soc. Am. **81**(5), 1609–1618 (1987).

[18] W. L. Griffith, R. Triolo, and A. L. Compere, "Analytical scattering function of a polydisperse Percus-Yevick fluid with Schulz distributed diameters," Phys. Rev. A **35**(5), 2200–2206 (1987).

[19] N. W. Ashcroft and J. Lekner, "Structure and resistivity of liquid metals," Physical Review **145**(1), 83–90 (1966).

[20] Anzivino C., Casiulis M., Zhang T., Moussa A. S., Martiniani S. and Zaccone A., "Estimating RCP in polydisperse and bidisperse hard spheres via an equilibrium model of crowding," J. Chem. Phys. **158**, 044901 (2023).

[21] O. Falou, M. Rui, A. E. Kaffas, J. C. Kumaradas, and M. C. Kolios, "The measurement of ultrasound scattering from individual micron-sized objects and its application in single cell scattering," J. Acoust. Soc. Am. **128**(2), pp. 894–902 (2010).

[22] M. F. Insana and T. J. Hall, "Parametric ultrasound imaging from backscatter coefficient measurements: Image formation and interpretation," Ultrason. Imag. **12**(4), 245–267 (1990).

[23] A. L. Gerig, T. Varghese, J. A. Zagzebski, "Improved parametric imaging of scatterer size estimates using angular compounding," IEEE Trans. on Ultrason. Ferroelect. Freq. Control **51**(6), 708–715 (2004).

[24] G. Ghoshal, M. L. Oelze, "Improved scatterer property estimates from ultrasound backscatter using gate-edge correction and a pseudo-Welch technique," IEEE Trans. on Ultrason. Ferroelect. Freq. Control **57**(12), 2828–2832 (2010).

[25] P. Muleki-Seya, R. Guillermin, J. Guglielmi, J. Chen, T. Pourcher, E. Konofagou, and E. Franceschini, "High frequency quantitative ultrasound spectroscopy of excised canine livers and mouse tumors using the structure factor model," IEEE Trans. on Ultrason., Ferroelect., Freq. Contr. **63**(9), 1335–1350 (2016).

[26] E. Franceschini, J.-M. Escoffre, A. Novell, L. Auboire, V. Mendes, Y. M. Benane, A. Bouakaz, and O. Basset, "Quantitative ultrasound in *ex vivo* fibrotic rabbit livers," Ultrasound Med. Biol. **45**(7), 1777–1786 (2019).

[27] A. Rohfritsch, E. Franceschini, A. Dupré, and D. Melodelima, "Quantitative ultrasound techniques for the assessment of thermal ablation: measurements of the backscatter coefficients from ex vivo human liver samples," Medical Physics **50**(11), 6908–6919 (2023).

[28] P. Muleki-Seya and W. D. O'Brien, "Ultrasound scattering from cell-pellet biophantoms and ex vivo tumors provides insight into the cellular structure involved in scattering," IEEE Trans. on Ultrason. Ferroelect. Freq. Control **69**(2), 637–649 (2022).